Research Paper

GEOSPHERE

GEOSPHERE, v. 16

https://doi.org/10.1130/GES02066.1

5 figures; 1 table; 1 supplemental file

CORRESPONDENCE: kmdenton@usgs.gov

CITATION: Denton, K.M., Ponce, D.A., Peacock, J.R, and Miller, D.M., 2019, Geophysical characterization of a Proterozoic REE terrane at Mountain Pass, eastern Mojave Desert, California, USA: Geosphere, v. 16, https://doi.org/10.1130/GES02066.1.

Science Editor: Shanaka de Silva
Associate Editor: Craig H. Jones

Received 21 September 2018
Revision received 14 September 2019
Accepted 31 October 2019

GOLD OPEN ACCESS

THE GEOLOGICAL SOCIETY OF AMERICA®

This paper is published under the terms of the CC-BY-NC license.

© 2019 The Authors

Geophysical characterization of a Proterozoic REE terrane at Mountain Pass, eastern Mojave Desert, California, USA

Kevin M. Denton, David A. Ponce, Jared R. Peacock, and David M. Miller

Geology, Minerals, Energy, and Geophysics Science Center, U.S. Geological Survey, Menlo Park, California 94025, USA

ABSTRACT

Mountain Pass, California (USA), located in the eastern Mojave Desert, hosts one of the world's richest rare earth element (REE) deposits. The REE-rich terrane occurs in a 2.5-km-wide, northwest-trending belt of Mesoproterozoic (1.4 Ga) stocks and dikes, which intrude a larger Paleoproterozoic (1.7 Ga) metamorphic block that extends ~10 km southward from Clark Mountain to the eastern Mescal Range. To characterize the REE terrane, gravity, magnetic, magnetotelluric, and whole-rock physical property data were analyzed. Geophysical data reveal that the Mountain Pass carbonatite body is associated with an ~5 mGal local gravity high that is superimposed on a gravity terrace (~4 km wide) caused by granitic Paleoproterozoic host rocks. Physical rock property data indicate that the Mountain Pass REE suite is essentially nonmagnetic at the surface with a magnetic susceptibility of 2.0×10^{-3} SI ($n = 57$), and lower-than-expected magnetizations may be the result of alteration. However, aeromagnetic data indicate that the intrusive suite occurs along the eastern edge of a distinct northwest-trending aeromagnetic high along the eastern Mescal Range. The source of this magnetic anomaly is ~1.5–2 km below the surface and coincides with an electrical conductivity zone that is several orders of magnitude more conductive than the surrounding rock. The source of the magnetic anomaly is likely a moderately magnetic pluton. Combined geophysical data and models suggest that the carbonatite and its associated REE-enriched ultrapotassic suite were preferentially emplaced along a northwest-trending zone of weakness, which has potential implications for regional mineral exploration.

INTRODUCTION

Carbonatite ore deposits are the primary source of rare earth elements (REEs), which are essential in modern civilian and military applications, healthcare and medical devices, and "green" technologies. Although REEs have crustal abundances similar to common industrial-grade metals (e.g., chromium, nickel, copper, zinc, tin, and lead), large economically viable REE deposits are uncommon (e.g., Haxel et al., 2002; Long et al., 2010; Verplanck and Van Gosen, 2011). The largest-known carbonatite-related REE deposit is in the Bayan Obo region of Inner Mongolia, China, and has produced ~97% of the global output of REEss (Haxel et al., 2002; Long et al., 2010; Hatch, 2012; Massari and Ruberti, 2013; U.S. Geological Survey, 2015). However, for several decades prior to the late 1980s, the Mountain Pass REE deposit in California, United States (Fig. 1), supplied much of the world's demand for industrial-grade REEs (Haxel et al., 2002; Castor, 2008).

A Proterozoic carbonatite terrane at Mountain Pass hosts the largest resource of light REEs in North America with proven reserves of ~16 million metric tons at an ore grade of ~8 wt% rare earth oxide (Castor, 2008; Mariano and Mariano, 2012). Since the discovery of the REE-bearing mineral bastnäsite in the carbonatite ore body in 1949, many studies have been carried out to investigate the occurrence, extent, and genesis of this REE deposit (e.g., Olson et al., 1954; Haxel, 2007; Poletti et al., 2016). Despite decades of research, the subsurface geology of this ore-bearing terrane remains largely unknown because previous studies have focused on its surface geology, geochemistry, and geochronology (e.g., Olson et al., 1954; Hewett, 1956; Burchfiel and Davis, 1971, 1988; DeWitt et al., 1987; Miller et al., 2007a; Haxel, 2007; Poletti et al., 2016).

Although geophysical studies have proven useful in understanding and constraining the geologic framework associated with REE deposits and their subsurface extent (e.g., McCafferty et al., 2014; Drenth, 2014; Shah et al., 2017), prior geophysical studies have primarily focused on localities adjacent to or outside the Mountain Pass area (e.g., Carlisle, 1982; Hendricks, 2007; Langenheim et al., 2009). In this study, we present new gravity (Denton and Ponce, 2016) and magnetotelluric (Peacock et al., 2019) data and interpretation for the Mountain Pass region. By integrating these new data sets with existing regional aeromagnetic (Kucks et al., 2006; Roberts and Jachens, 1999) and local geologic and structural data (Olson et al., 1954; Hewett, 1956; Burchfiel and Davis, 1988; Fleck et al., 1994; Castor, 2008), we produce detailed geophysical maps and models of the subsurface related to the Mountain Pass REE terrane. Our contribution helps elucidate the regional geologic framework at Mountain Pass by characterizing regional geologic structures in the subsurface that may have influenced the emplacement of the REE-enriched intrusive suite.

GEOLOGIC BACKGROUND

The Mountain Pass REE terrane is located in the eastern Mojave Desert near the California-Nevada border (Fig. 1A). This terrane lies along the central portion of a northwest-trending mountain belt that includes, from north to south, the Clark Mountain Range, Mohawk Hill, Mescal Range, and Ivanpah Mountains. This mountain belt is bounded by Shadow Valley to the west and Ivanpah

Downloaded from https://pubs.geoscienceworld.org/gsa/geosphere/article-pdf/doi/10.1130/GES02066.1/4907657/ges02066.pdf
by guest

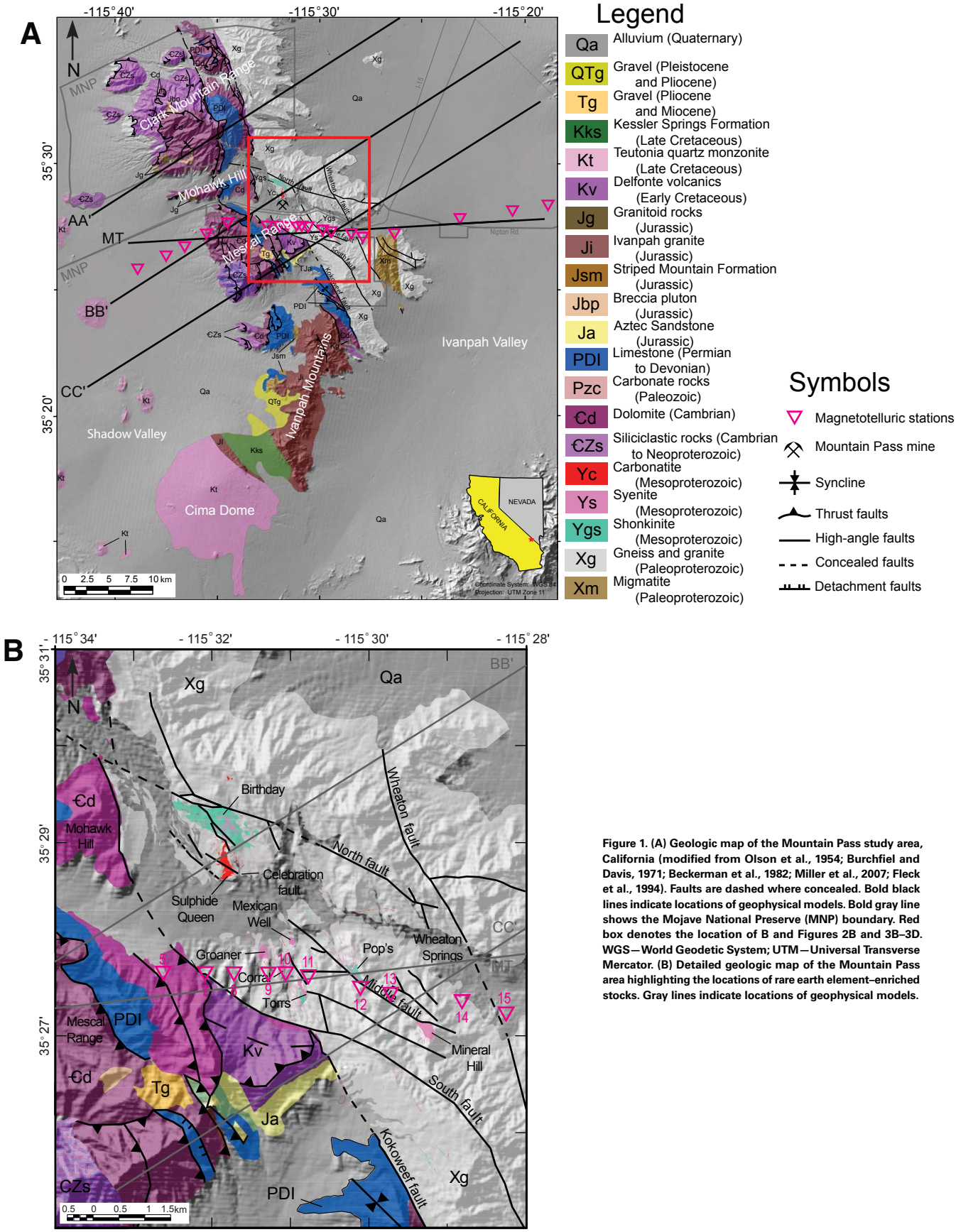


Figure 1. (A) Geologic map of the Mountain Pass study area, California (modified from Olson et al., 1954; Burchfiel and Davis, 1971; Beckerman et al., 1982; Miller et al., 2007; Fleck et al., 1994). Faults are dashed where concealed. Bold black lines indicate locations of geophysical models. Bold gray line shows the Mojave National Preserve (MNP) boundary. Red box denotes the location of B and Figures 2B and 3B–3D. WGS—World Geodetic System; UTM—Universal Transverse Mercator. (B) Detailed geologic map of the Mountain Pass area highlighting the locations of rare earth element–enriched stocks. Gray lines indicate locations of geophysical models.

Downloaded from https://pubs.geoscienceworld.org/gsa/geosphere/article-pdf/doi/10.1130/GES02066.1/4907657/ges02066.pdf
by guest

Valley to the east. The western section of the mountain belt is composed of Neoproterozoic to early Paleozoic carbonates and metasedimentary rocks, and Mesozoic silicic volcanic and plutonic rocks that are thrusted against autochthonous Paleoproterozoic crystalline basement rocks to the east (Burchfiel and Davis, 1971, 1988). The metamorphic basement rocks are primarily gneiss and schist and compose the eastern section of the mountain belt (Fig. 1A; Hewett, 1956; Burchfiel and Davis, 1971, 1988; Wooden and Miller, 1990).

At Mountain Pass, REE enrichment has been identified in tabular to oblate sill-like stocks of variable composition and numerous dikes and veins within the Paleoproterozoic basement rocks (Fig. 1B; Olson et al., 1954; Haxel, 2007). These Mesoproterozoic REE-enriched intrusions are localized along a narrow northwest-trending zone, following the regional foliation of the host gneiss (Olson et al., 1954; Hewett, 1956), and extend discontinuously from the southern base of the Clark Mountain Range south to the northern foothills of the Ivanpah Mountains. Rock types associated with the REE suite consist of shonkinite, syenite, and granite, as well as the Sulphide Queen carbonatite ore body (Fig. 1B; Olson et al., 1954; DeWitt et al., 1987; Haxel, 2007). Although variable REE enrichment has been observed in these rocks, only the Sulphide Queen carbonatite at Mountain Pass has been proven economically viable (Castor, 1991, 2008; Castor and Hedrick, 2006; Haxel, 2007; Theodore, 2007).

Field relationships and early radiometric dating document complex spatial and temporal associations between the ultrapotassic suite and the carbonatite, but their similar geochemical characteristics led previous workers to suggest derivation from a common parental melt (e.g., Olson et al., 1954; Woyski, 1980; Castor, 2008). More recent geochronologic, geochemical, and isotopic data (e.g., Premo et al., 2013; Poletti et al., 2016) suggest that the carbonatite and ultrapotassic suite are primary mantle melts that were generated separately from the same source region. Radiometric dating of the ultrapotassic suite suggests that emplacement occurred in three phases at ca. 1.425, ca. 1.405, and ca. 1.380 Ga and that emplacement of the carbonatite body was coeval with the latter two stages (Poletti et al., 2016).

Several subparallel faults cut the Mountain Pass area in proximity to the REE-enriched outcrops and include the NNW-striking Kokoweef fault, the northwest-striking South, Middle, North faults, and the previously unmapped NNW-striking Wheaton faults (Fig. 1B; Olson et al., 1954; Walker et al., 1995). Despite sparse exposures, it has been determined that faults in general dip steeply (~70°) to the southwest, but style and orientation are variable (Burchfiel and Davis, 1988; Davis et al., 1993; Walker et al., 1995). Offset indicators along many of these faults are rare but are generally thought to indicate mostly left-lateral motion (Hewett, 1956).

The NNW-striking Kokoweef fault (also referred to as the southern extent of the Clark Mountain fault by Hewett, 1956) is a normal or left-lateral fault (Hewett, 1956; Burchfiel and Davis, 1971) that extends at least 9.5 km from its southern exposure in the northeastern Ivanpah Mountains to its northern termination in the eastern Mescal Range (Fig. 1). Fault rocks include ductile phyllonite and breccia with chlorite, hematite, and sericite alteration. Paleoproterozoic basement gneiss (unit Xg) to the east is juxtaposed against Paleozoic carbonate rocks (units ЄZs, Єd, PDl), Mesozoic sandstone (unit Ja), and volcanic rocks (unit Kv) to the west (Fig. 1; Hewett, 1956; Fleck et al., 1994; Walker et al., 1995). The carbonate rocks along the Kokoweef fault trace are offset by ~300 m (Hewett, 1956).

At its northern extent, the Kokoweef fault is intersected by the WNW-striking South fault, which bends prominently to the west and constitutes a bounding structure of the Mescal Range (Fig. 1). Units are truncated and downdropped to the southwest where the two faults converge. The South fault carries similar alteration assemblages to those found in the Kokoweef fault but includes additional fault materials and rocks, such as gouge and breccia, but lacks phyllonite. Both the Kokoweef and South faults truncate ca. 100 Ma volcanic rocks (unit Kv in Fig. 1A) and are therefore considered some of the youngest faults in the area (Fig. 1B; Fleck et al., 1994; Walker et al., 1995). North of the South fault–Kokoweef fault convergence, the South fault cuts eastern Mohawk Hill as a thrust fault just west of the Sulphide Queen carbonatite body as part of the Mesozoic fold-and-thrust belt (Fig. 1B; Burchfiel and Davis, 1971).

The northwest-striking Middle fault was mapped by Olson et al. (1954) as an ~3-km-long linear trace that begins west of Mineral Hill, continues through the western edge of Pop's stock (also referred to as the "Wheaton" stock by Haxel [2007]) and extends northwestward to Mexican Well before it is concealed by Quaternary alluvial deposits (Fig. 1B). It is unclear whether the Middle fault continues northwest along this trend and joins the Celebration fault, a northwest-striking fault with apparent left-lateral offset that cuts the Sulphide Queen ore body.

The northwest-striking North fault is a left-lateral strike-slip fault that extends for at least 8 km and may continue northwest of Mountain Pass (Fig. 1B). The fault cuts metamorphic basement rocks just north of Wheaton Springs and traverses discontinuously until passing only a few meters north of the Birthday shonkinite body at Mountain Pass. Olson et al. (1954, p. 27) reported "considerable" displacement and an abrupt truncation of the Birthday stock and associated dikes along the North fault. The North fault continues northeast ~0.5 km beyond Mountain Pass, where it is concealed by shallow alluvium before its trace reemerges north of the Mohawk Hill summit (Miller et al., 2007a). Both the North and Middle faults have alteration assemblages similar to those associated with the South fault as well as breccia and gouge fault materials.

The NNW-striking Wheaton fault zone extends for ~15 km east of the South, Middle, and North faults (Fig. 1A; Olson et al., 1954). Fault exposures are limited but consist of closely spaced fractures, shear zones, and gouge and vary in width from ~10 m wide in the south to 300-m-wide zones east of Mineral Hill (Fig. 1B). The Wheaton fault generally strikes NNW (315°) and dips steeply (~70°) to the southwest, however structural complexities are observed at its northern extent where the North fault bends into and joins the Wheaton fault zone. Although several Paleoproterozoic rock units are present on both sides of the Wheaton fault (Fig. 1A; units Xg and Xm), distinctive trondhjemite-tonalite complexes are known only northeast of the fault (Fig. 1). The fault zone may have offset Paleoproterozoic rocks significantly, but shonkinite dikes present on both sides of the fault indicate limited offset since Mesoproterozoic time. Wall-rock alteration along the fault zone is characterized by limonite, chlorite,

Downloaded from https://pubs.geoscienceworld.org/gsa/geosphere/article-pdf/doi/10.1130/GES02066.1/4907657/ges02066.pdf
by guest

sericite, and hematite mineralization that is cut by silica veins. The Wheaton fault is similar to the Kokoweef fault in that early ductile rock fabric (phyllonite) is overprinted by chlorite and sericite alteration and breccia.

GEOPHYSICAL METHODS

Gravity Data

Detailed gravity surveys were conducted throughout the study area to supplement existing data (Ponce, 1997; Langenheim et al., 2009), and data were collected at >2300 stations (Denton and Ponce, 2016) in areas of poor control, with station spacing ranging from ~100 to 400 m (Fig. 2). Raw gravity measurements were processed using standard gravity reduction methods (e.g., Blakely, 1995) to produce isostatic anomaly values. Data reduction includes terrain corrections (Godson and Plouff, 1988), which remove the effect of topography, and isostatic corrections (Simpson et al., 1986), which remove long-wavelength variations in the gravity field related to compensation of topographic loads. For additional details of the processing of these data, see Denton and Ponce (2016). These reduction methods are used to produce isostatic gravity anomalies that reflect the density variations of sources in the middle to upper crust (Fig. 2). Gravity data were gridded at a 100 m interval, and horizontal gradients were calculated to emphasize lateral variations in density and to highlight the edges of gravity sources (e.g., Blakely and Simpson, 1986).

Aeromagnetic Data

Aeromagnetic data were derived from statewide compilations for California (Roberts and Jachens, 1999) and Nevada (Kucks et al., 2006). Individual surveys were flown at various flight-line elevations and spacings, thus aeromagnetic data were either upward or downward continued to a constant elevation of 305 m above the ground, adjusted to a common datum, and merged to produce a uniform magnetic anomaly map (Fig. 3A; Roberts and Jachens, 1999; Kucks et al., 2006). This compilation allows for seamless interpretation of magnetic anomalies across survey boundaries. Widely spaced surveys or those flown at higher flight-line elevations may lack the resolution to resolve shallow magnetic sources in some parts of the study area. However, these issues are not significant for the generalized and regional-scale magnetic interpretations presented in this study.

We applied a reduction-to-pole (RTP) transformation to the existing aeromagnetic data to remove the influence of the Earth's magnetic field (e.g., declination = 11.6°; inclination = 61°) on the anomalies (Fig. 3; Baranov, 1957; Baranov and Naudy, 1964). Maximum horizontal gradients (MHGs) were then calculated to highlight variations in magnetization that characterize source features such as structural boundaries and faults (Figs. 3; Blakely and Simpson, 1986; Grauch and Cordell, 1987; Blakely, 1995). The separation of magnetic signals from different sources at varying depths was accomplished by applying a matched filtering technique (Figs. 3C and 3D; Syberg, 1972; Phillips, 2001).

Magnetotelluric Data

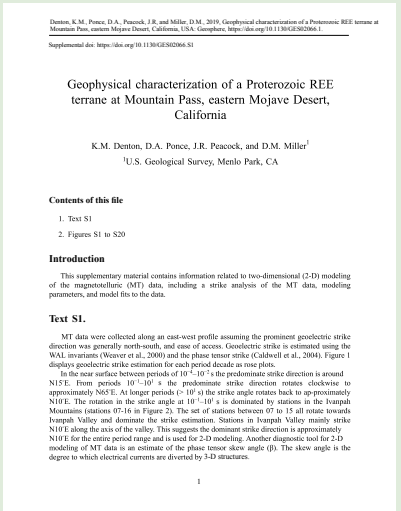
Magnetotellurics (MT) is an electromagnetic method that is typically employed for investigating deep (10 km or more) subsurface resistivities and is especially sensitive to fluids or hydrothermal mineralization in geologic structures (e.g., Peacock et al., 2015). Electrical conductivity is commonly attributed to enhanced porosity and permeability that creates high fluid connectivity. Fluid-filled interconnected pore spaces can increase the overall bulk-rock conductivity of subsurface features by orders of magnitude (Olhoeft, 1985), creating a strong contrast with resistive basement rocks.

MT data were collected at 18 locations using equipment developed by Zonge International (Fig. 1; Peacock et al., 2019). Station spacing varied from ~1 to 5 km along profile MT in Figure 1A, with closer spacing near the Mountain Pass district. Individual MT stations were deployed along Interstate Highway 15 and continuing east along Nipton Road, perpendicular to the regional strike of the mountain ranges, establishing a profile. The MT system consisted of a ZEN 32-bit data logger, four ANT-4 induction coils (1000–0.001 Hz), and Borin Ag-AgCl electrodes. At each station, instrumentation was set up in a cross pattern, with four electrodes spaced 50 m apart from the data logger, and recorded for ~20 h. Vertical magnetic fields were not collected due to difficulty of burying a vertical induction coil.

Frequency-dependent MT transfer functions were estimated using Zonge International processing software, and synchronous stations were used as remote references to reduce noise (Gamble et al., 1979). All collected time series of electrical and magnetic data were processed in the frequency domain using Fourier transforms to estimate the impedance tensor (see Supplemental Figs. S1–S20[1]), which contains frequency and directional information related to the regional resistivity structure and electrical response of the subsurface for modeling (Kunetz, 1972).

2-D Geophysical Models

Geophysical models were constructed along three parallel, northeast-trending profiles approximately perpendicular to the regional geologic strike (Fig. 1) using gridded gravity and aeromagnetic data and GM-SYS (Geosoft software) for simultaneous gravity and magnetic two-dimensional (2-D) and 2½-dimensional (2.5-D) forward modeling (Fig. 4). An MT model was constructed along an east-west profile. Profiles AA′, CC′, and MT were modeled in 2-D, whereas profile BB′ was modeled in 2.5-D to incorporate off-axis source bodies associated with REE intrusions (Fig. 4; unit Yc). Model depths extend to ~6 km for gravity and magnetic models and ~20 km for the MT model (Figs. 4 and 5). Model depth extent is based in part on the resolution of the potential field



Denton, K.M., Ponce, D.A., Peacock, J.R., and Miller, D.M., 2019, Geophysical characterization of a Proterozoic REE terrane at Mountain Pass, eastern Mojave Desert, California, USA: Geosphere, https://doi.org/10.1130/GES02066.1.

Supplemental doi: https://doi.org/10.1130/GES02066.S1

Geophysical characterization of a Proterozoic REE terrane at Mountain Pass, eastern Mojave Desert, California

K.M. Denton, D.A. Ponce, J.R. Peacock, and D.M. Miller[1]

[1]U.S. Geological Survey, Menlo Park, CA

Contents of this file

1. Text S1
2. Figures S1 to S20

Introduction

This supplementary material contains information related to two-dimensional (2-D) modeling of the magnetotelluric (MT) data, including a strike analysis of the MT data, modeling parameters, and model fits to the data.

Text S1.

MT data were collected along an east-west profile assuming the prominent geoelectric strike direction was generally north-south, and ease of access. Geoelectric strike is estimated using the WAL invariants (Weaver et al., 2000) and the phase tensor strike (Caldwell et al., 2004). Figure 1 displays geoelectric strike estimation for each period decade as rose plots.

In the near surface between periods of 10^{-1}–10^{-3} s the predominate strike direction is around N15°E. From periods 10^{-1}–10^{1} s the predominate strike direction rotates clockwise to approximately N65°E. At longer periods (> 10^{1} s) the strike angle rotates back to up-proximately N10°E. The rotation in the strike angle at 10^{-1}–10^{1} s is dominated by stations in the Ivanpah Mountains (stations 07-16 in Figure 2). The set of stations between 07 to 15 all rotate towards Ivanpah Valley and dominate the strike estimation. Stations in Ivanpah Valley mainly strike N10°E along the axis of the valley. This suggests the dominant strike direction is approximately N10°E for the entire period range and is used for 2-D modeling. Another diagnostic tool for 2-D modeling of MT data is an estimate of the phase tensor skew angle (β). The skew angle is the degree to which electrical currents are diverted by 3-D structures.

1

[1]Supplemental Material. Information related to two-dimensional (2-D) modeling of magnetotelluric (MT) data, including: strike analysis, modeling parameters, and model fits to the data. Please visit https://doi.org/10.1130/GES02066.S1 or access the full-text article on www.gsapubs.org to view the Supplemental Material.

Downloaded from https://pubs.geoscienceworld.org/gsa/geosphere/article-pdf/doi/10.1130/GES02066.1/4907657/ges02066.pdf
by guest

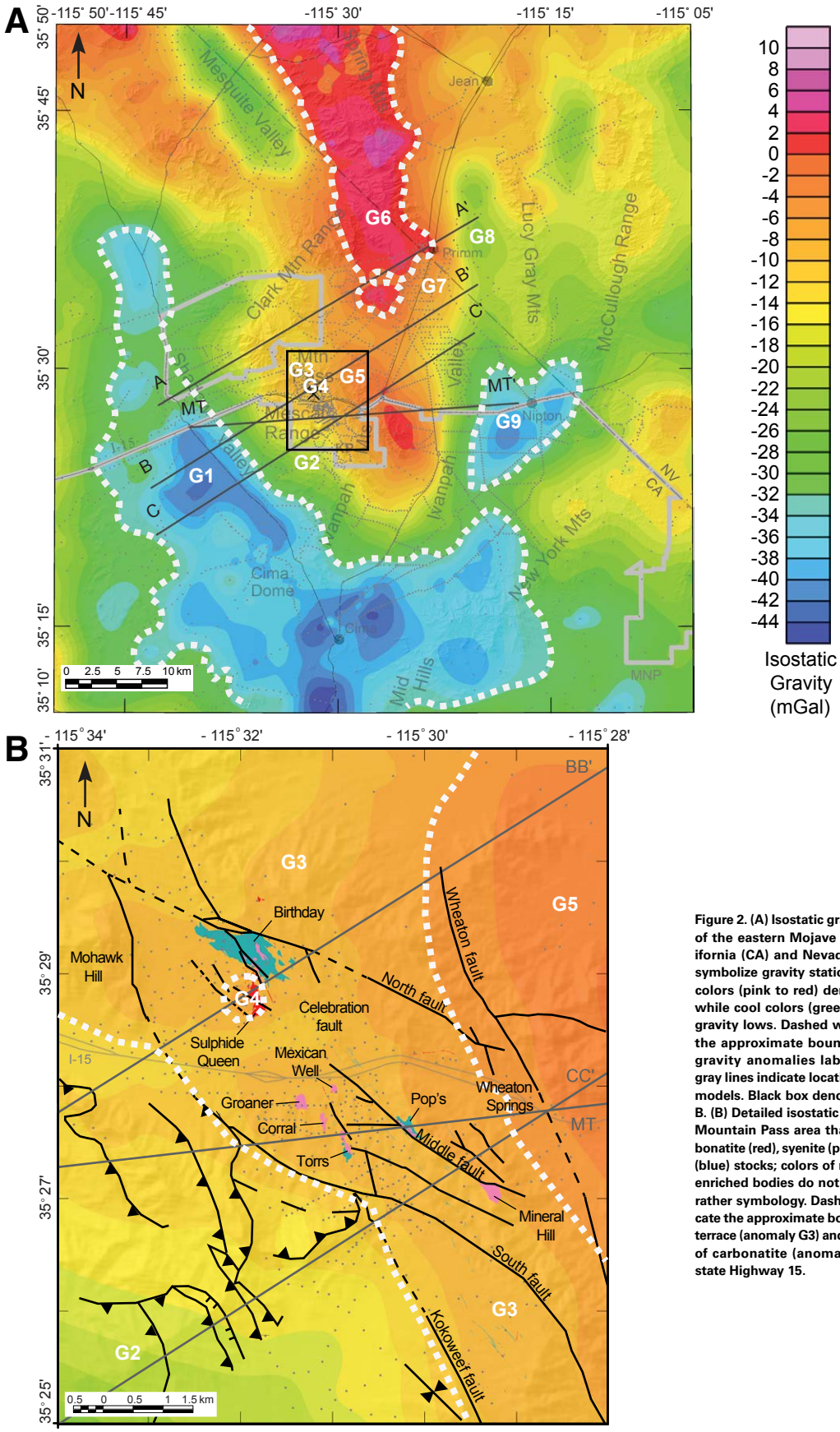


Figure 2. (A) Isostatic gravity anomaly map of the eastern Mojave Desert region, California (CA) and Nevada (NV). Gray dots symbolize gravity station locations. Warm colors (pink to red) denote gravity highs, while cool colors (green to blue) indicate gravity lows. Dashed white lines indicate the approximate boundaries of regional gravity anomalies labeled G1–G9. Dark gray lines indicate locations of geophysical models. Black box denotes the location of B. (B) Detailed isostatic gravity map of the Mountain Pass area that includes the carbonatite (red), syenite (pink), and shonkinite (blue) stocks; colors of rare earth element–enriched bodies do not reflect density but rather symbology. Dashed white lines indicate the approximate boundaries of gravity terrace (anomaly G3) and gravity expression of carbonatite (anomaly G4). I-15—Interstate Highway 15.

Downloaded from https://pubs.geoscienceworld.org/gsa/geosphere/article-pdf/doi/10.1130/GES02066.1/4907657/ges02066.pdf
by guest

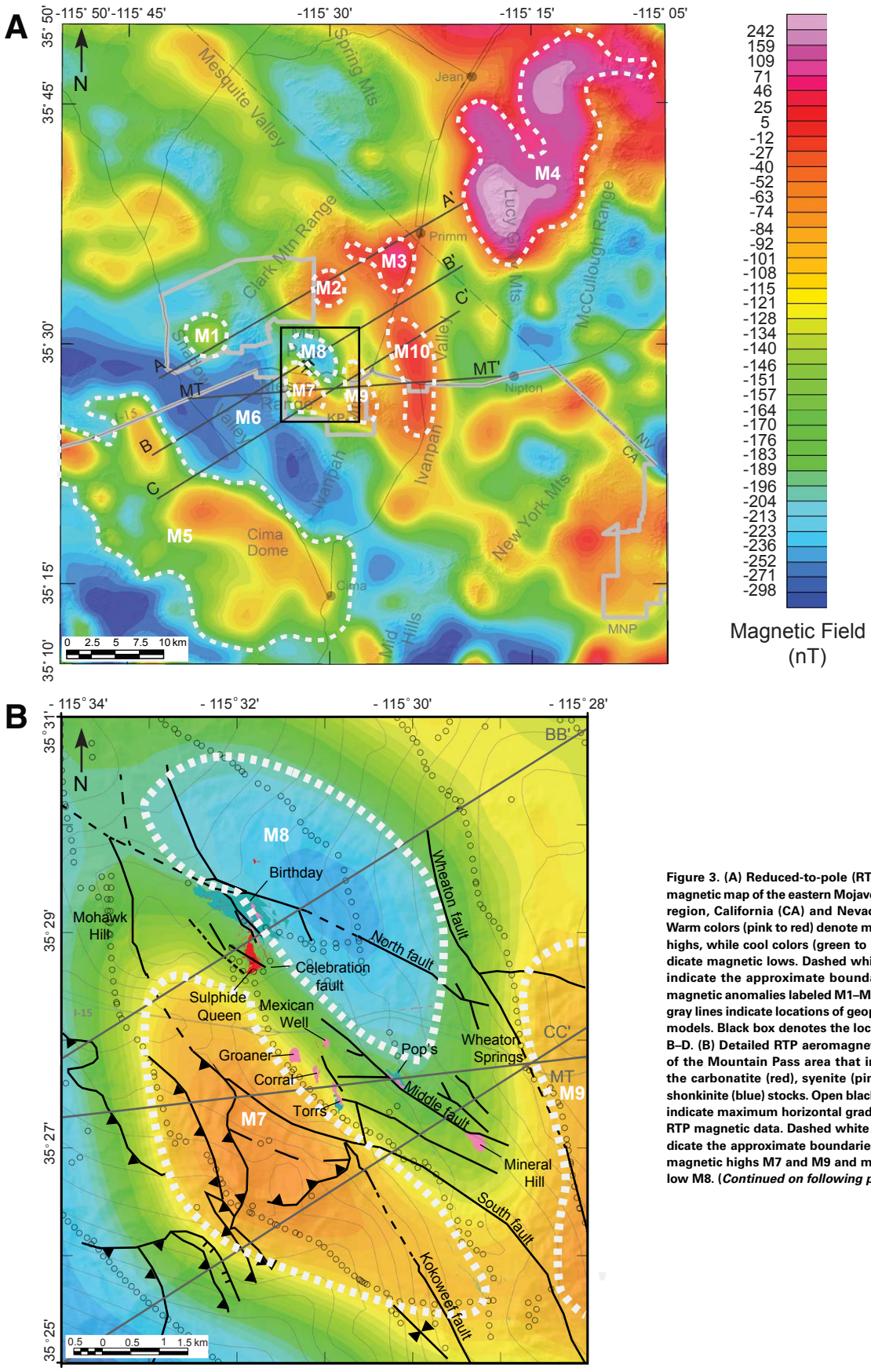


Figure 3. (A) Reduced-to-pole (RTP) aeromagnetic map of the eastern Mojave Desert region, California (CA) and Nevada (NV). Warm colors (pink to red) denote magnetic highs, while cool colors (green to blue) indicate magnetic lows. Dashed white lines indicate the approximate boundaries of magnetic anomalies labeled M1–M10. Dark gray lines indicate locations of geophysical models. Black box denotes the location of B–D. (B) Detailed RTP aeromagnetic map of the Mountain Pass area that includes the carbonatite (red), syenite (pink), and shonkinite (blue) stocks. Open black circles indicate maximum horizontal gradients of RTP magnetic data. Dashed white lines indicate the approximate boundaries of the magnetic highs M7 and M9 and magnetic low M8. (*Continued on following page.*)

Downloaded from https://pubs.geoscienceworld.org/gsa/geosphere/article-pdf/doi/10.1130/GES02066.1/4907657/ges02066.pdf
by guest

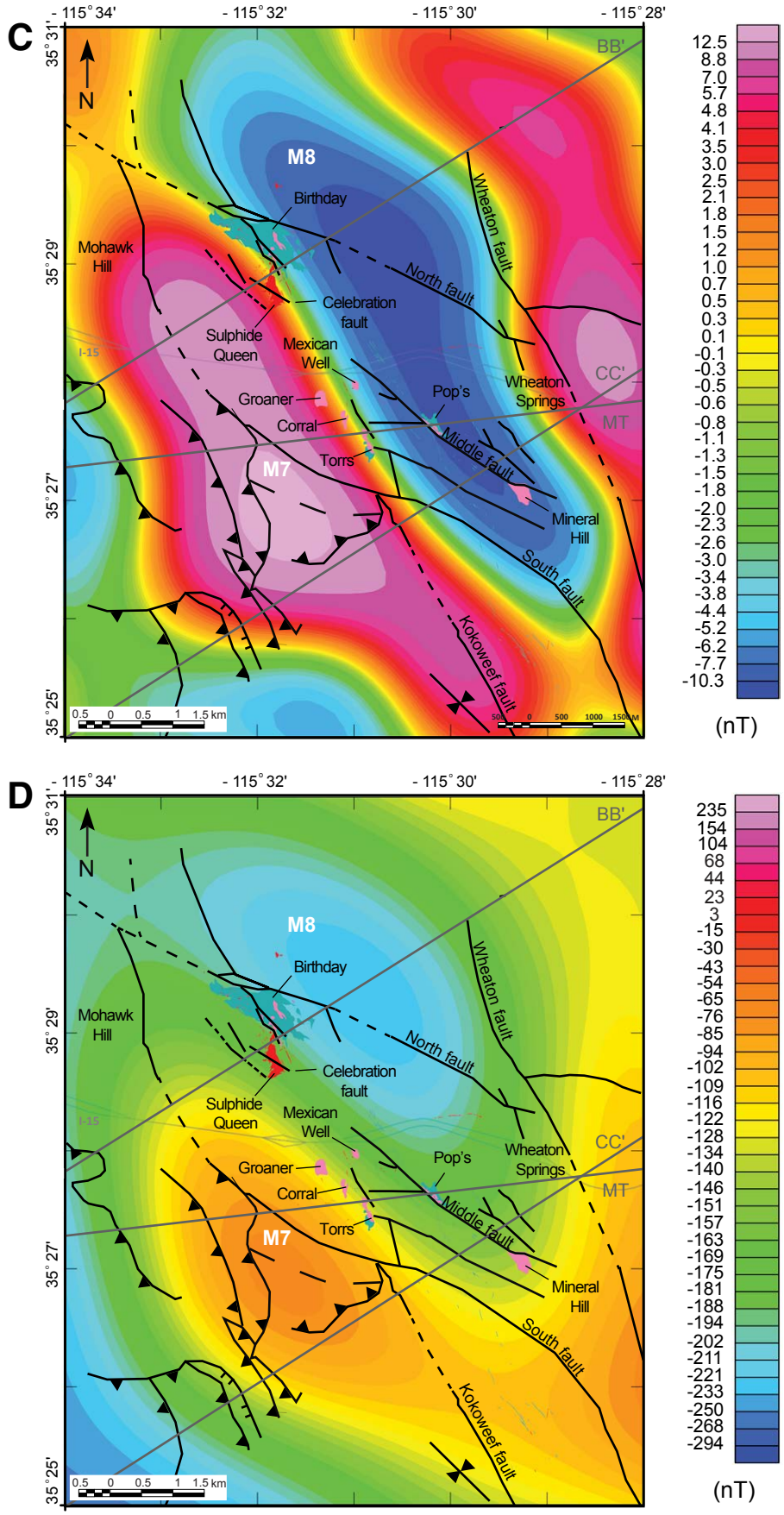


Figure 3 (*continued*). (C) Matched filtered aeromagnetic map corresponding to an equivalent dipole layer at an intermediate depth of 2.4 km. (D) Matched filtered aeromagnetic map corresponding to an equivalent half space at the deepest equivalent layer at a depth of 4.3 km. I-15—Interstate Highway 15.

Downloaded from https://pubs.geoscienceworld.org/gsa/geosphere/article-pdf/doi/10.1130/GES02066.1/4907657/ges02066.pdf
by guest

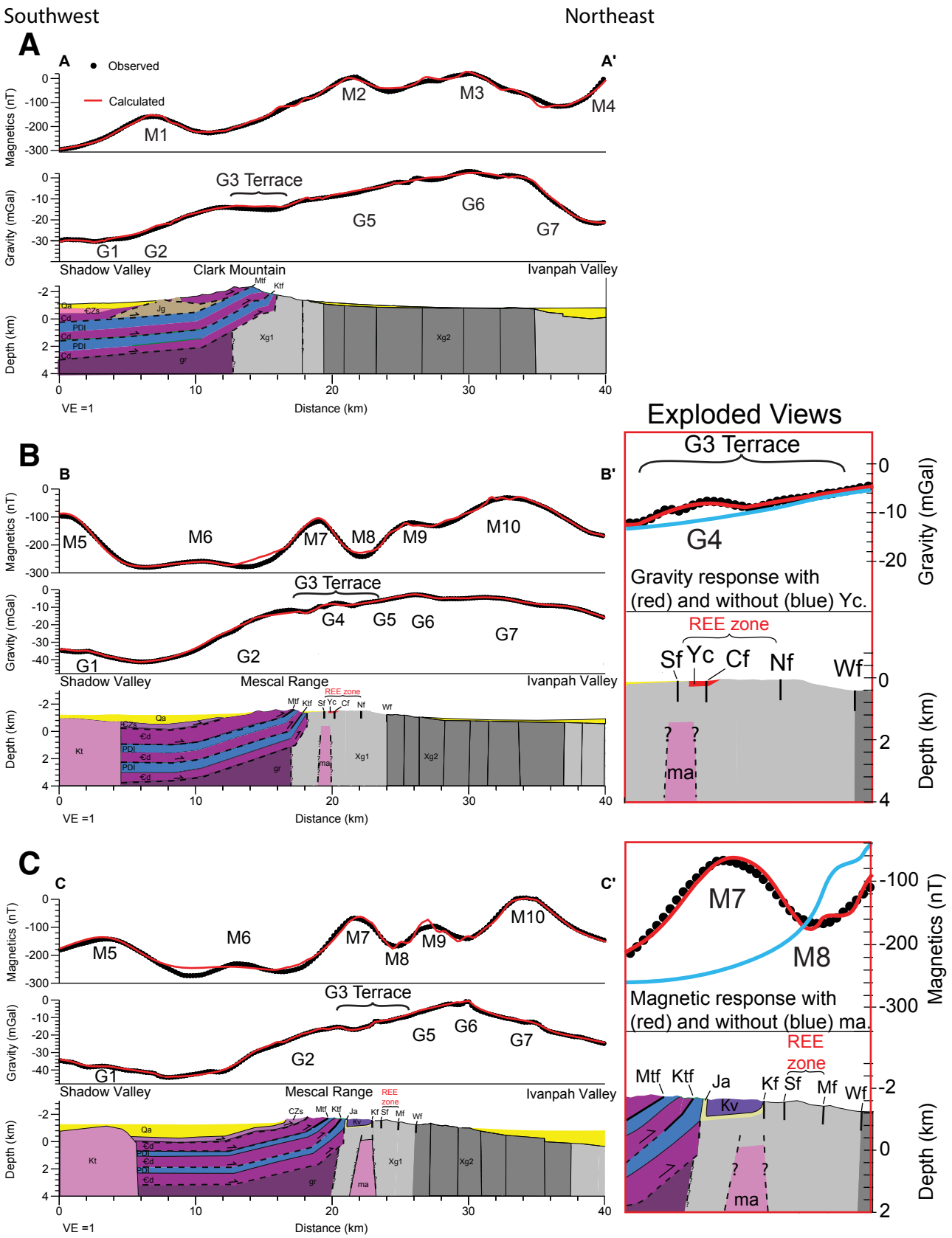


Figure 4. Two-dimensional (A and C) and 2½-dimensional (B) forward gravity, magnetic, and geologic models for the Mountain Pass region, California, including exploded views of B and C, showing the carbonatite body (unit Yc) and inferred pluton (body ma). Gravity (G1–G7) and magnetic (M1–M10) anomalies are indicated. Faults are denoted as follows: Mtf—Mesquite Pass thrust fault; Ktf—Keaney–Mollusk Mine thrust fault; Sf—South fault; Cf—Celebration fault; Kf—Kokoweef fault; Mf—Middle fault; Nf—North fault; Wf—Wheaton faults. Refer to Figure 1 for location and geologic explanation and Table 1 for model attributes. Note, unit Qa is alluvium. REEs—rare earth elements; VE—vertical exaggeration.

Downloaded from https://pubs.geoscienceworld.org/gsa/geosphere/article-pdf/doi/10.1130/GES02066.1/4907657/ges02066.pdf
by guest

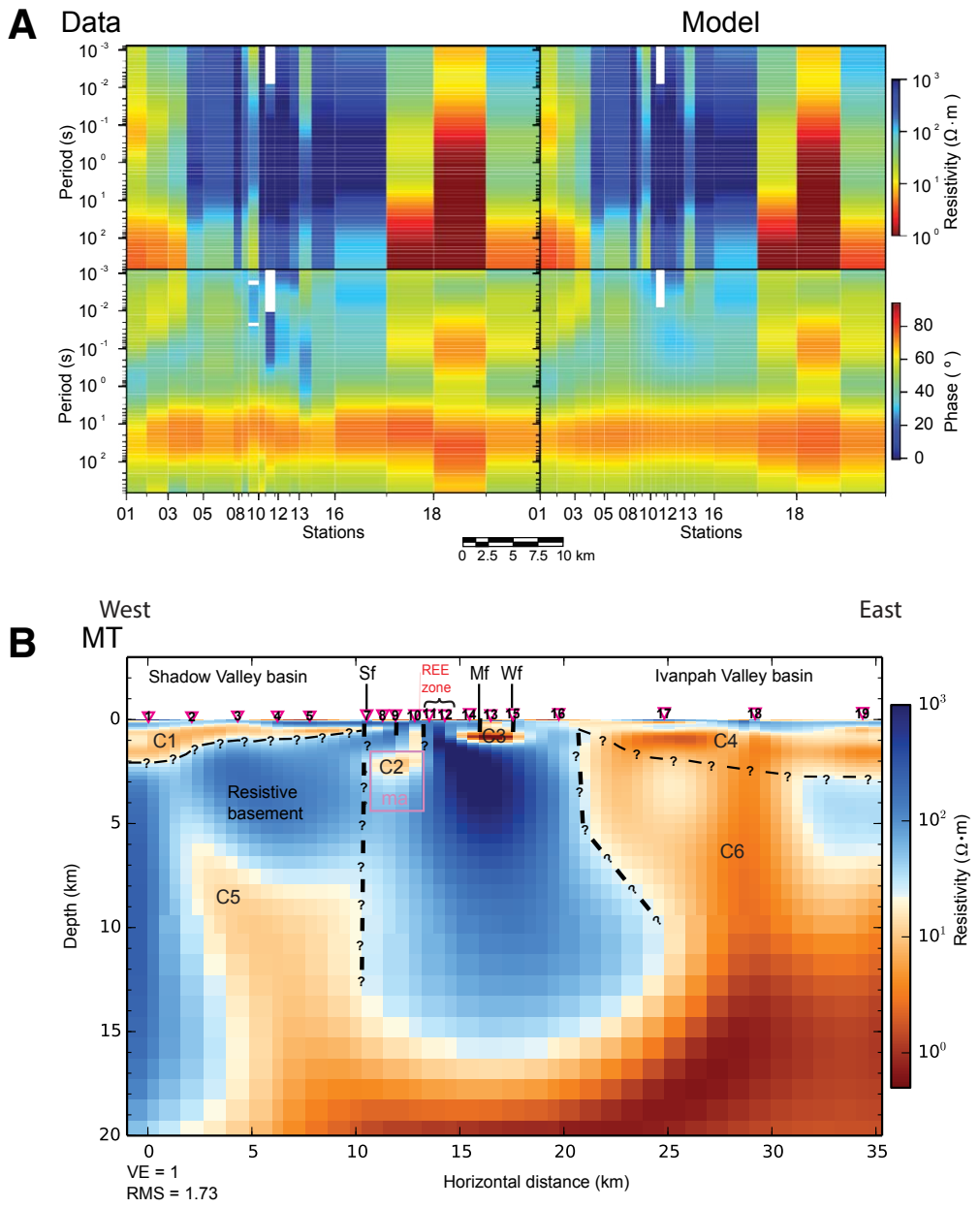


Figure 5. (A) Psuedosection of the magnetotelluric (MT) data used for the inversion (top) and the preferred resistivity model MT response (bottom), Mountain Pass region, California. White color represents no data. (B) Two-dimensional resistivity model along profile MT (see Fig. 1 for location). Warm colors (orange to red) denote conductive features, whereas cool colors (purple to blue) denote resistive features. Conductive features are denoted as anomalies C1–C6. Geologic faults are denoted as follows: Sf—South fault; Mf—Middle fault; Wf—Wheaton fault. Geologic contacts are dashed where inferred. Approximate boundaries of inferred magnetic pluton (body ma) is outlined in pink. See Supplemental Material (text footnote 1) for additional MT analysis, modeling parameters, and model fits to data (Peacock et al., 2019). REE—rare earth element; VE—vertical exaggeration; RMS—root mean square.

Downloaded from https://pubs.geoscienceworld.org/gsa/geosphere/article-pdf/doi/10.1130/GES02066.1/4907657/ges02066.pdf
by guest

data and the depth of geologic features that include: regional basins <2 km deep (Langenheim et al., 2009), pluton and basement exposures (Miller et al., 2007a), and velocity-model estimates of Moho depths <30 km (Tape et al., 2012).

Additional modeling considerations were based on the capabilities of each applied technique for boundary and depth detection of sources. For example, gravity and magnetic methods are ideal for upper and middle crustal depths and edge detection of dense and magnetic sources (Blakely, 1995). MT applications are excellent complements to gravity and magnetic techniques, particularly in imaging of deep structures in geologically complex areas, and provides inferences on the presence of fluids and mineralogical domains in mid- to lower-crustal depths of resistivity sources for this study (Wannamaker, 2005).

Models were constrained by combining gravity, magnetic, and MT data, geologic mapping and cross sections (Hewett, 1956; Olson et al., 1954; Burchfiel and Davis, 1988; Wooden and Miller, 1990; Fleck et al., 1994), drill-hole information (Castor, 2008; Langenheim et al., 2009), rock-property data (Denton and Ponce, 2016), and depth-to-basement estimates (Langenheim et al., 2009). In the models, source bodies are assumed to have uniform average densities and magnetic susceptibility values that are derived from physical property measurements of rock samples from the study area (Table 1; Denton and Ponce, 2016). Combined, these constraints dramatically reduce the ambiguity and nonuniqueness inherent in geophysical models. Although potential-field modeling is nonunique, the final models are based on numerous iterations (>30 per model) and testing to produce geologically reasonable models (Saltus and Blakely, 2011). A simple block model approach is taken for regional structural complexities (e.g., Mesozoic thrusting of Paleozoic sections), whereas more effort is made to highlight local Proterozoic structure and details associated with subsurface geology and framework related to the northwest-trending REE terrane at Mountain Pass (Fig. 1B).

Magnetotelluric model inversions were used to estimate resistivity structures using a 2-D Occam inversion code (deGroot-Hedlin and Constable, 1990). The data were rotated to the predominant geoelectric strike direction N10°E as estimated from the phase tensor strike angle (Caldwell et al., 2004). Station locations were projected onto a profile line striking N100°E. The modeling grid consists of 144 × 100 mesh cells, where cell width is 250 m and cell depth increases logarithmically downward such that the total model size is 150 × 300 km to avoid edge effects (Fig. 5A). Only the transverse magnetic (TM) mode was used for inversion to reduce the influence of three-dimensional bodies (Wannamaker et al., 1984). Multiple starting models and resistivity structures were tested to ensure robustness. The preferred model has a normalized root-mean-square error of 1.73 using only the TM mode with an error floor of ~20% for the apparent resistivity and an error floor of 1.4° for the impedance phase (Peacock et al., 2016). The data and model response fits are shown in Figure 5A, where the model represents the data well with only a few exceptions. The model has difficulty representing short periods of stations 11–15, which is likely due to noise from the nearby mine (Figs. 5A–5B). For additional details regarding the inversion process and modeling, see the Supplemental Material (footnote 1) for strike analysis and model fits (Supplemental Figs. S1–S20).

Table 1. Physical Properties of Geologic Units in Models

Unit	Description	Density (kg/m^3)	Magnetic Susceptibility (SI)
ma	magnetic rock	2650	0.040
gr	granitic rock	2640	0
QTa	Alluvial sediments (Quaternary and Tertiary)	2000	0
Kt	Teutonia adamellite (Cretaceous)	2640	0.010
Kv	Volcanic rocks (Cretaceous)	2550	0
Jg	Granitoid rocks (Jurassic)	2590	0.005
Ja	Aztec Sandstone (Jurassic)	2530	0
PDl	Limestone (Permian to Devonian)	2600	0
Ꞓd	Dolomite (Cambrian)	2700	0
ꞒZs	Siliciclastic (Cambrian to Neoproterozoic)	2400	0
Yc	Carbonatite (Mesoproterozoic)	3000	0
Xg2	Gneiss, granite, and amphibolite (Paleoproterozoic)	2700	0.008-0.014
Xg1	Gneiss and granite (Paleoproterozoic)	2600	0

Physical properties based on Denton and Ponce (2016).

INTERPRETIVE RESULTS

Regional Geophysics

The geologic framework of the region is revealed in the isostatic gravity and magnetic anomaly maps of the Mountain Pass area (Figs. 2A and 3A, respectively). Regional anomalies reflect the orientation of the major geologic units and structures of the region (Hewett, 1956; Burchfiel and Davis, 1971; Miller et al., 2007). In general, gravity highs represent denser metamorphic basement rocks (anomaly G6 in Fig. 2), whereas gravity lows represent relatively less-dense

Downloaded from https://pubs.geoscienceworld.org/gsa/geosphere/article-pdf/doi/10.1130/GES02066.1/4907657/ges02066.pdf
by guest

basin fill and granitic basement (anomaly G1). For example, gravity highs over the northwest-trending mountain ranges (Spring Mountains, Clark Mountain Range, Mescal Range, and the northern Ivanpah Mountains) are associated with relatively dense Paleozoic dolomitic rocks (units ЄZs, Єd) and Proterozoic gneissic basement rocks (unit Xg). In contrast, a prominent gravity low in Shadow Valley (anomaly G1) corresponds to ~1 km of basin fill at its maximum depth (Fig. 4; Langenheim et al., 2009) and the likely presence of exposed Cretaceous Teutonia batholith granite (unit Kt) at Cima Dome in southern Shadow Valley (Figs. 1 and 2A). High-amplitude and moderate-wavelength magnetic anomalies characterize the moderately magnetic unit Kt (anomaly M5 in Fig. 3A).

A moderate gravity high (anomaly G8) over the northern extent of Ivanpah Valley is primarily produced by shallowly concealed, moderately dense, gneissic basement (Fig. 2A). A gravity low (anomaly G9) over the central extent of the valley (near Nipton) reflects a thickening accumulation of basin sediment, which agrees with seismic studies (Carlisle, 1982). A series of high-amplitude (>100 nT) magnetic highs (anomalies M3 and M10) occur along the entire north-south gravity gradient (anomaly G7) of Ivanpah Valley, which may be related to relatively magnetic plutons and/or dikes within the gneissic basement (Fig. 3A).

Mountain Pass Intrusive Suite

The carbonatite and associated intrusive suite at Mountain Pass form a belt of eight REE-enriched stocks (Figs. 1B) that lies within a gravity terrace (Fig. 2B, anomaly G3) and along the eastern edge of a prominent magnetic anomaly (Fig. 3B, anomaly M7). The ~4-km-wide gravity terrace probably reflects lower-density and nonmagnetic Paleoproterozoic granodiorite gneiss that is bound to the west by the South and Kokoweef faults and to the east by the Wheaton fault. The source of the magnetic high (anomaly M7) adjacent to the REE intrusive suite is inferred to be pluton not exposed at the surface (Figs. 3A–3B). MHGs and matched filtering of magnetic data suggest that the top of the inferred pluton is at a depth of ~1.5–2 km and occupies an ~3-km-wide zone that extends ~5 km southeast beneath portions of the eastern Mescal Range (Figs. 3B–3D).

The Sulphide Queen carbonatite ore body is associated with a relative ~5 mGal gravity high (Fig. 2B, anomaly G4) that is superimposed on a gravity terrace (anomaly G3). Physical-property data show that the barite-bastnäsite–rich carbonatite is very dense and essentially nonmagnetic (Denton and Ponce, 2016). The carbonatite has an average saturated bulk density of 2993 kg/m^3 with a range of 2440–3591 kg/m^3 and an average magnetic susceptibility 0.18×10^{-3} with a range of 0.03–0.61×10^{-3} SI (Denton and Ponce, 2016). The carbonatite forms a west-southwest moderately dipping (~40°) body (Olson et al., 1954; Castor, 2008) that terminates near the gradient that marks the eastern edge of the northwest-trending aeromagnetic high (Figs. 3A–3D, anomaly M7).

Shonkinite, syenite, and alkali granite rocks, associated with the Mountain Pass REE belt, produce weak gravity anomalies relative to the gravity terrace (Fig. 2B, anomaly G3) and are essentially nonmagnetic (Figs. 3B–3D; Table 1). Physical rock property data for shonkinite rocks collected at the Birthday, Torrs, and Pop's stocks have an average saturated bulk density of 2834 kg/m^3 with a range of 2647–3000 kg/m^3 and an average magnetic susceptibility 0.11×10^{-3} with a range of 0.07–4.45×10^{-3} SI (Denton and Ponce, 2016). Syenite and alkali granites collected at the Groaner, Corral, Torrs, Pop's (no alkali granite at this location), and Mineral Hill areas have relatively lower densities than shonkinite or carbonatite. Syenite rocks have saturated bulk densities of 2670 kg/m^3 with a range of 2555–2788 kg/m^3 and an average magnetic susceptibility 3.47×10^{-3} with a range of 0.19–11.46×10^{-3} SI (Denton and Ponce, 2016). Alkali granites have saturated bulk densities of 2617 kg/m^3 with a range of 2541–2704 kg/m^3 and an average magnetic susceptibility 0.82×10^{-3} with a range of 0.01–3.44×10^{-3} SI (Denton and Ponce, 2016).

The MT data reveal a highly conductive (low-resistivity) zone (Fig. 5B, anomaly C2) coincident with the upper portion (~1.5–2 km depth) of the inferred pluton (Fig. 3, anomaly M7), which is several orders of magnitude (10^3) more conductive than the surrounding rocks (Fig. 5B). If the upper portion of the inferred pluton were mineralized or fractured and fluid filled, this would account for the observed high conductivities. Alternatively, sulfide mineralization associated with the nearby Sulphide Queen gold mine at Mountain Pass (Hewett, 1956; Olson et al., 1954), for which the Sulphide Queen carbonatite ore body is named (Olson, et al., 1954), could account for these high conductivities adjacent to the REE intrusive suite.

Modeling Descriptions and Interpretations

2-D Model AA′

The northernmost profile AA′ is an ~40-km-long northeast-trending transect that stretches from Shadow Valley across the southern Clark Mountain Range and California-Nevada state line to northern Ivanpah Valley (Fig. 1). Model AA′ (Fig. 4A) highlights the low-angle, west-dipping regional structures of the Mesozoic Clark Mountain thrust complex to the west that are juxtaposed against the Proterozoic gneissic basement blocks that are exposed in the Mountain Pass area and underlie the wide Ivanpah Valley alluvial basin. Shadow Valley is characterized by <1 km of Cenozoic alluvial fill (unit Qa), similar to findings of Langenheim et al. (2009). The fill is underlain by a thick section of Paleozoic carbonates and siliciclastic rocks (units ЄZs, Єd, PDl) and moderately dense and nonmagnetic granitic basement (Figs. 2 and 4A, anomaly G1 and body gr). The western margin of the Clark Mountain Range corresponds to a circular, low-amplitude magnetic anomaly (Fig. 3A, anomaly M1) that may represent a decapitated granitic Jurassic pluton (unit Jg). Termination of relatively dense Paleozoic rocks and granitic basement against exposures of relatively less-dense Proterozoic granitic gneiss along the western part of the Clark Mountain Range produces a flattening or terracing of the gravity field (anomaly G3), a general feature that appears in all gravity models but is widest along this profile (Figs. 2 and 4A).

High-amplitude gravity and magnetic anomalies (Figs. 2A and 3A, anomalies G6 and M2, M3, M9, M10) occurring west of Ivanpah Valley probably

Downloaded from https://pubs.geoscienceworld.org/gsa/geosphere/article-pdf/doi/10.1130/GES02066.1/4907657/ges02066.pdf
by guest

reflect a relatively denser and more-magnetic mafic gneiss. Alternatively, these anomalies have amplitudes consistent with mafic amphibolite veins and dikes that intrude gneissic exposures east of Mineral Hill area (Fig. 3B, anomaly M9). The model terminates just west of the highly magnetic 1.65–1.68 Ga Lucy Gray pluton (Almeida et al., 2016), which produces the most prominent magnetic anomaly (Fig. 3A, anomaly M4) in the study area (Figs. 3A and 4A). The Lucy Gray pluton was modeled just off the end of the profile to match the upward gradient at the end of the profile.

2.5-D Model BB′

Profile BB′ stretches from Shadow Valley just south of Interstate 15, across the Mescal Range and the Sulphide Queen carbonatite ore body, and beyond the eastern flank of Clark Mountain to Ivanpah Valley just east of the California-Nevada state line (Fig. 1). Model BB′ is a 2.5-D model that highlights the geophysical expression of the Sulphide Queen carbonatite REE mineral deposit and important structural features related to the Mountain Pass area (Fig. 4B, unit Yc).

Based on model BB′, Cretaceous quartz monzonite of the Teutonia batholith (unit Kt) extends at least to a depth of ~4 km immediately below the western margin of the Shadow Valley basin. Modeling and physical property data (Denton and Ponce, 2016) reveal that the geophysical signature of unit Kt is less prominent than that of older metasedimentary units (ЄZs, PDl, Єd) in the region (Fig. 4B; Table 1). In addition, unit Kt is moderately magnetic, producing a pronounced magnetic anomaly (M5) relative to surrounding nonmagnetic basement rocks. Unit Kt's moderately magnetic character differentiates it from other granitic plutons (e.g., unit Ji and body gr) and carbonate rocks in the area (Figs. 1A and 4B). A thick, dipping section of dense and mostly nonmagnetic Paleozoic metasedimentary, carbonate, and siliciclastic units, along with concealed basement rocks, is the source of the steep gravity gradient (anomaly G2) and the low magnetic response (anomaly M6) over the eastern part of Shadow Valley and western part of the Mescal Range (Fig. 4B).

The geometry of the Sulfide Queen carbonatite ore body is based on surface mapping and drill-hole data (Olson et al., 1954; Castor, 2008; Castor and Nason, 2004; Denton and Ponce, 2016). The carbonatite is ~200 m wide and ~250 m thick along profile BB′ and is modeled as a tabular body that dips ~30°–35°SW. The resulting model supports a relatively small but dense carbonatite body that likely extends ~250–300 m to the southwest, terminating near the northeastern edge of the M7 anomaly at the steepest edge of the gradient as defined by maximum horizontal gradients (Fig. 3B).

The carbonatite body is proximal to several northwest-striking, left-lateral faults that include the South fault to the southwest, Celebration fault which directly cuts through the carbonatite body, and the North fault just to the northeast. Some of these faults are truncated to the east by the previously unmapped Wheaton fault to the east (Figs. 1B and 4B). While it is difficult to directly attribute specific geophysical gradient responses along profile to individual fault expressions, the Wheaton fault zone in general occurs within unit Xg1 and the defined bounding edges of the G3 gravity terrace (Fig. 2B). Proterozoic granitic gneissic basement rocks that are present throughout Mountain Pass produce a flattening or terracing (anomaly G3) of the gravity field along an ~4-km-wide northwest-trending zone (Fig. 4). However, denser carbonatite (unit Yc) intruding the gneissic basement superimposes a local ~5 mGal gravity anomaly (anomaly G4) onto the gravity terrace (anomaly G3), producing a relatively small response or "bump" on the gravity terrace (Fig. 4B). The G4 gravity anomaly produced is clearly associated with the exposed and known extent of the carbonatite body, as no other geologic feature has the needed density (3000 kg/m^3) to account for this gravity anomaly (Table 1). The source of the magnetic anomaly M7 (Fig. 4B, body ma) adjacent to the carbonatite body and REE suite is uncertain; it is not associated with an appreciable gravity anomaly, therefore it must be of relatively low density and thus cannot represent the carbonatite body. A likely candidate for this relatively low-density and moderately magnetic body is a granitic intrusion.

2-D Model CC′

The southernmost profile CC′ stretches from the western edge of Shadow Valley, crossing the southern Mescal Range and the northern Ivanpah Mountains, to Ivanpah Valley, just west of the California-Nevada border (Fig. 1A). Model CC′ (Fig. 4C) reveals an overall southward thickening of the basin fill (unit Qa) beneath both Shadow and Ivanpah Valleys relative to other model profiles, which is consistent with regional depth-to-basement estimates (Langenheim et al., 2009). The prominent magnetic anomaly M7 (Fig. 3B) observed in model BB′ extends southeast at least 5 km to model CC′, and its eastern gradient delineates the westernmost extent of the REE intrusive suite and roughly bounds an ~4-km-wide zone of unit Xg1 that contains the Kokoweef, South, Middle, and Wheaton faults. Additionally, matched filtering of magnetic data indicates that the source of the M7 magnetic high is ~1.5–2 km below the surface (Figs. 3B–3D), the top of which coincides with a moderately strong electrically conductive feature (Fig. 5B; body ma). Model CC′ reveals that the source of anomaly M7 is not unique to profile BB′ and demonstrates its key role in understanding the spatial trend and structural relationship of not just the carbonatite, but the associated REE intrusive suite.

2-D Model MT

Magnetotelluric model MT (Fig. 5B) is ~45 km long and trends east-west from the central part of Shadow Valley across Mountain Pass and adjacent Nipton Road (Fig. 1). In general, basement rocks (e.g., unit Kt, body gr, and unit Xg) in the study area are electrically resistive, as their crystalline structures make them less porous, reducing the ability for ions to move and electrically conduct. In contrast, basin-fill sediments shed from nearby ranges are composed of

Downloaded from https://pubs.geoscienceworld.org/gsa/geosphere/article-pdf/doi/10.1130/GES02066.1/4907657/ges02066.pdf
by guest

calcareous sediment, quartz grains, and clay-rich sands and gravels that are more porous with high potential for fluid retention, which could explain their high conductivities. However, resistivities in the upper ~500 m in Shadow Valley and upper 1 km in Ivanpah Valley are imaged to be on the order of 50–100 Ω·m. Well data in the area (maximum depth ~300 m) measures water resistance to be on the order of 100–10,000 Ω (Moyle, 1972), which supports freshwater fluids within the upper parts of the basin. Unfortunately, there are no well data to support porosity estimates, but if a two-phase modified Archie's equation is considered to estimate porosity (Glover, 2010), assuming the resistivity of the basin fill is on the order of 20–50 Ω·m with a cementation factor of two and fresh water (1000 Ω·m) in the pore space, porosity is estimated to be between 5%–15%. The lower parts of the basin are conductive, suggesting increases in pore-space salinity with lower porosity, on the order of 1%–5%. The upper more-resistive parts of the basin suggest basin depths consistent with regional depth-to-basement estimates by Langenheim et al. (2009) (Fig. 5B, anomalies C1 and C4).

Shadow Valley appears as a wedge-shaped conductive feature that tapers to the east near the base of the Mescal Range, which is consistent with the gravity and magnetic profiles (Fig. 4B). The MT model indicates that conductive basin fill for Shadow Valley is as deep as ~1–1.5 km near its western extent and shallows toward the eastern range front (Fig. 5B). The Cima volcanic field located at the southwestern margin of Shadow Valley represents late Cenozoic eruptions (<11,600 yr B.P. in age), which suggest an active or cooling magmatic source beneath part of the basin (Phillips, 2003). Hydrothermal fluids associated with the Cima volcanic system might be contributing to the electrical conductivity at depth (Fig. 5B, anomaly C5) as reported in nearby Basin and Range settings (Wannamaker et al., 2008).

Similarly, the lower extent of Ivanpah Valley is also conductive (anomaly C4) and produces a strongly defined gradient along its western edge, however its depth is complicated by a highly conductive zone (anomaly C6) beneath Ivanpah Valley, likely caused by deeper geologic structures (Fig. 5B). Ivanpah Valley is ~150 to 300 m lower in elevation than Shadow Valley and could serve as a drain for the regional watershed, with increased hydrologic interaction between surface and groundwater fluids that likely contributes to its conductivity at depth. However, conductive feature C6 continues to depths of as much as 20 km, which is unlikely to be solely attributable to enhanced penetration of meteoric waters (Fig. 5B). Conductive anomalies along Ivanpah Valley could reflect a more complex network that could reflect associations with brecciated plutons, concealed faulting, mineralization, or possibly alteration by hydrothermal fluids (Figs. 4–5, anomalies C4 and C6). Based on the proximity of the Cima volcanic field system, it is conceivable that conductive fluids and evaporates from this magmatic system could contribute to the conductivity beneath Ivanpah Valley. While MT data are limited, evidence supports interconnected sources at depth (>15 km) between prominent conductors (Fig. 5B, anomalies C5 and C6), suggesting a possible adjoining structure (Fig. 5B).

Perhaps the most significant feature in the MT model related to the Mountain Pass REE zone is a shallow (~1.5–2 km) conductive feature (~10^1 Ω·m) adjacent to the Sulphide Queen carbonatite ore body (Fig. 5B, anomaly C2). This ~3-km-wide conductive feature is about three orders of magnitude more conductive than the surrounding rocks and is likely cut by the inferred trace of the Kokoweef and/or South faults. While its spatial extent is not well constrained beyond this MT profile, C2 is well constrained just west of known REE bodies and correlates well with the prominent magnetic high (anomaly M7) along both models BB′ and CC′. Finally, areas spanning the Middle and Wheaton faults are conductive (anomaly C3), suggesting that sections of the REE suite as mapped by Olson et al. (1954) may be conductive and possibly fault controlled.

DISCUSSION AND CONCLUSIONS

In general, carbonatites and their associated REE terranes have distinct gravity and magnetic signatures because they are relatively dense and commonly contain magnetite or are associated with magnetic rocks (e.g., Ramberg, 1973; Dindi and Swain, 1988; Ray and Lefebure, 2000; Groves and Vielreicher, 2001; Drenth, 2014). Interestingly, the REE suite at Mountain Pass, California, is essentially nonmagnetic (Denton and Ponce, 2016). In addition, the surrounding Proterozoic host rocks and younger Paleozoic rocks in the nearby ranges are also essentially nonmagnetic, with a few exceptions that include amphibolite rocks and small dikes and veins of fine-grained shonkinite (Denton and Ponce, 2016).

Although the carbonatite ore body and other 1.4 Ga REE rocks (shonkinite, syenite, and granite) are essentially nonmagnetic, they occur along the eastern margin of a northwest-trending prominent magnetic (Fig. 3, anomaly M7) and conductive (Fig. 5, anomaly C2) anomalies. The steep magnetic gradient (between anomalies M7 and M8) coincides with the eastern edge of the inferred pluton (Figs. 4 and 5, body ma) and likely represents a preferential zone of weakness and/or a fault. East of this inferred pluton, a broad magnetic low (anomaly M8) may reflect the absence of magnetic rocks near the surface and an accommodation zone for REE mineralization. We suggest that if the pluton (body ma) is older than the 1.4 Ga intrusive suite, the REE intrusive suite may have been preferentially emplaced along a preexisting feature or fault zone. However, if the pluton was concurrent with or younger than the 1.4 Ga intrusive suite, then perhaps the pluton preferentially intruded along a zone weakened by the older intrusive suite rocks.

The magnetic high (anomaly M7) near the western edge of the REE suite, as delineated by anomaly maps (Fig. 3A), RTP and MHG filtering (Figs. 3B–3D), and modeling (Figs. 4B–4C and 5), probably reflects a magnetic intrusive body rather than a REE-related deposit, because the latter would be nonmagnetic (Figs. 3B–3D; Table 1). Our preferred interpretation is that the REE suite lies within a steep gradient (anomalies M7 and M8) that likely highlights a concealed northwest-striking contact or fault. The proximity of the magnetic low (anomaly M8) raises the possibility that a hydrothermal or magmatic event(s) has altered the magnetic minerals within the rocks of the Mountain Pass locality.

Downloaded from https://pubs.geoscienceworld.org/gsa/geosphere/article-pdf/doi/10.1130/GES02066.1/4907657/ges02066.pdf
by guest

While RTP filtering of magnetic data mostly removes the possibility of anomalies M7 and M8 being a dipole feature, the magnetic low (M8) could be a relatively lower-amplitude anomaly between two adjacent magnetic highs (Fig. 3B, anomalies M7 and M9).

However, alteration is well documented (Shawe, 1953; Wooden and Miller, 1990; Haxel, 2007; Premo et al., 2013; Stoeser, 2013; Poletti et al., 2016) in the region, as geologic mapping indicates that the central corridor of the carbonatite terrane resides in a zone of alteration (Olson et al., 1954). Outside this zone are moderately to strongly magnetic (~0.5% magnetite) mafic rocks, gneisses, and amphibolite rocks that are also relatively dense (Table 1, unit Xg2). Geochronological (Premo et al., 2013) and geochemical (Stoeser, 2013) data suggest that the 1.4 Ga REE intrusive suite exhibits widespread hydrothermal alteration and/or multiple stages of alteration or magmatism (Shawe, 1953; Poletti et al., 2016). Alteration and magmatic events could also explain some of the unusual geochemical features of the REE suite, including extremely elevated enrichment of incompatible elements (Castor, 2008) and the apparent age gaps between intrusion of the carbonatite (1375 ± 7 Ma, DeWitt et al., 1987; 1396 ± 16 and 1371 ± 10 Ma, Poletti et al., 2016) and the ultrapotassic rocks (1410 ± 7 to 1400 ± 8 Ma: DeWitt et al., 1987; 1.417 ± 5 Ga: Premo et al., 2013; 1429 ± 10 to 1385 ± 18 Ma: Poletti et al., 2016). Multiple thermal alteration events may have affected not only the Proterozoic rocks in the Mountain Pass area, but the Music Valley (near Joshua Tree National Park ~220 km south-southwest) REE terrane as well: both areas experienced at least two distinct thermal and/or fluid-related alteration events, with the oldest dated at ca. 1.71 and 1.4 Ga, the latter associated with REE mineralization (McKinney et al., 2015).

In conclusion, geophysical results indicate that the entire REE intrusive suite is located within a gravity terrace (Figs. 2 and 4, anomaly G3) and east of a prominent magnetic feature (Figs. 3 and 4, anomaly M7) and a conductive anomaly (Fig. 5B, anomaly C2). The source of anomalies M7 and C2 has a sharply defined geometry, with a top that probably occurs at a depth of ~1.5–2 km and extending >4 km based on matched filtering of magnetic data and geophysical modeling (Figs. 3, 4, and 5). The gravity terrace (anomaly G3) is defined by steep, northwest-trending gravity gradients and is bounded by the Clark Mountain and South-Kokoweef faults to the west and near the Wheaton fault to the east (Fig. 2). The gravity terrace reflects relatively lower-density granitic gneiss (e.g., unit Xg1) and other granitic intrusive rocks (e.g., units Ji, Kt) present in models AA′–CC′ (Fig. 4; Table 1). The source of the magnetic anomaly (M7) shown in models BB′ and CC′ is a relatively low-density and moderately magnetic intrusive granitic pluton (body ma) that is not exposed at the surface and is spatially associated with the 1.4 Ga Mountain Pass terrane.

Combined geophysical and geologic investigations of the eastern Mojave Desert carbonate terrane provide new insights into the structural framework of the Mountain Pass REE deposit. This geophysical study of the eastern Mojave Desert carbonatite terrane demonstrates the effectiveness of a multi-technique approach to studying the supporting structures that host REE deposits in the Mountain Pass area. Finally, future studies of Mountain Pass would benefit from high-resolution airborne geophysical surveys capable of continuous data gathering over much broader regions to include coverage of rugged and otherwise inaccessible mountain ranges. For example, high-resolution aeromagnetic, gravity gradiometry, lidar (light detection and ranging), and radiometric data would be ideal for evaluating the region in greater detail. In addition, better understanding of faulting, structural analysis, and kinematics associated with 1.4 Ga structures would dramatically improve the overall constraints and insights related to the REE mineralization in the Mojave Desert.

ACKNOWLEDGMENTS

This work was funded by the Mineral Resources Program of the U.S. Geological Survey. We would like to thank John Landreth, Daniel Cordier, and Brittany Frolick of Molycorp Minerals, LLC.; Doug Davis and Amanda Shieb of the Ivanpah Solar Thermal Facility; and David Nichols and Debra Hughson of the Mojave National Preserve for facilitating our field efforts. We also thank Bruce Chuchel, Clay Jernigan, Carson MacPherson-Krutsky, and Ben Flanagan for field support. Reviews by Victoria Langenheim, Stephen Park, and an unnamed reviewer greatly improved the manuscript. Special thanks to *Geosphere* staff and editors Gina Harlow, Craig Jones, and Shanaka de Silva for editorial support.

Any mention by this study of any private or commercial entity or use of related products (e.g., GM-SYS, Geosoft, Zonge International, ZEN 32-bit data logger, ANT-4 induction coils) is in no way an endorsement or commitment of any kind by the U.S. Government, U.S. Geological Survey, or any affiliated government agency.

REFERENCES CITED

Almeida, R.V., Cai, Y., Hemming, S.R., Christie-Blick, N., and Neiswanger, L.S., 2016, Reexamination of the crustal boundary context of Mesoproterozoic granites in southern Nevada using U-Pb zircon chronology and Nd and Pb isotopic compositions: The Journal of Geology, v. 124, p. 313–329, https://doi.org/10.1086/685766.

Baranov, V., 1957, A new method for interpretation of aeromagnetic maps: Pseudo-gravimetric anomalies: Geophysics, v. 22, p. 359–382, https://doi.org/10.1190/1.1438369.

Baranov, V., and Naudy, H., 1964, Numerical calculation of the formula of reduction to the magnetic pole: Geophysics, v. 29, p. 67–79, https://doi.org/10.1190/1.1439334.

Beckerman, G.M., Robinson, J.P., and Anderson, J.L., 1982, The Teutonia batholith: A large intrusive complex of Jurassic and Cretaceous age in the eastern Mojave Desert, California, *in* Frost, E.G., and Martin, D.L., eds., Mesozoic-Cenozoic Tectonic Evolution of the Colorado River Region, California, Arizona, and Nevada—Anderson-Hamilton Volume: San Diego, Cordilleran Publishers [in conjunction with a symposium and field trip for the Geological Society of America], p. 205–221.

Blakely, R.J., 1995, Potential Theory in Gravity and Magnetic Applications: New York, Cambridge University Press, 441 p., https://doi.org/10.1017/CBO9780511549816.

Blakely, R.J., and Simpson, R.W., 1986 Approximating edges of source bodies from magnetic or gravity anomalies: Geophysics, v. 51, p. 1494–1498, https://doi.org/10.1190/1.1442197.

Burchfiel, B.C., and Davis, G.A., 1971, Clark Mountain thrust complex in the Cordillera of southeastern California: Geologic summary and field trip guide, *in* Elders, W.A., ed., Geological Excursions in Southern California: Riverside, University of California, Campus Museum Contribution 1, p. 1–28.

Burchfiel, B.C., and Davis, G.A., 1988, Mesozoic thrust faults and Cenozoic low-angle normal faults, eastern Spring Mountains, Nevada, and Clark Mountains thrust complex, California, *in* Weide, D.L., and Faber, M.L., eds., This Extended Land—Geological Journeys in the Southern Basin and Range: Geological Society of America Cordilleran Section Field Trip Guidebook: University of Nevada Geoscience Department Special Publication 2, p. 87–105.

Caldwell, T.G., Bibby, H.M., and Brown, C., 2004, The magnetotelluric phase tensor: Geophysical Journal International, v. 158, p. 457–469, https://doi.org/10.1111/j.1365-246X.2004.02281.x.

Carlisle, C.L., 1982, The subsurface structure of the Ivanpah Valley, California, as determined by geophysical measurements [M.S. thesis]: Santa Barbara, University of California, 90 p.

Castor, S.B., 1991, Rare earth deposits in the southern Great Basin, *in* Raines, G.L., Lisle, R.E., Schafer, R.W., and Wilkinson, W.H., eds., Geology and Ore Deposits of the Great Basin: Symposium Proceedings: Reno, Geological Society of Nevada, v. 1, p. 523–528.

Downloaded from https://pubs.geoscienceworld.org/gsa/geosphere/article-pdf/doi/10.1130/GES02066.1/4907657/ges02066.pdf
by guest

Castor, S.B., 2008, The Mountain Pass rare earth carbonatite and associated ultrapotassic rocks, California: Canadian Mineralogist, v. 46, p. 779–806, https://doi.org/10.3749/canmin.46.4.779.

Castor, S.B., and Hedrick, J.B., 2006, Rare earth elements, *in* Kogel, J.E., Trivedi, N.C., Barker, J.M., and Krukowski, S.T., eds., Industrial Minerals and Rocks: Commodities, Markets, and Uses (seventh edition): Littleton, Colorado, Society for Mining, Metallurgy, and Exploration, p. 759–792.

Castor, S.B., and Nason, G.W., 2004, Mountain Pass rare earth deposit, California, *in* Castor, S.B., Papke, K.G., and Meeuwig, R.O., eds., Betting on Industrial Minerals: Proceedings of the 39th Forum on the Geology of Industrial Minerals, Reno-Sparks, Nevada, May 18–24, 2003: Nevada Bureau of Mines and Geology Special Publication 33, p. 58–81.

Davis, G.A., Fowler, T.K., Bishop, K.M., Brudos, T.C., Friedman, S.J., Burbank, D.W., Parke, M.A., and Burchfiel, B.C., 1993, Pluton pinning of an active Miocene detachment fault system, eastern Mojave Desert, California: Geology, v. 21, p. 627–630, https://doi.org/10.1130/0091-7613(1993)021<0627:PPOAAM>2.3.CO;2.

deGroot-Hedlin, C., and Constable, S., 1990, Occam's inversion to generate smooth, two-dimensional models from magnetotelluric data: Geophysics, v. 55, p. 1613–1624, https://doi.org/10.1190/1.1442813.

Denton, K.M., and Ponce, D.A., 2016, Gravity and magnetic studies of the eastern Mojave Desert, California and Nevada: U.S. Geological Survey Open-File Report 2015-1070, 20 p., https://doi.org/10.3133/ofr20161070.

DeWitt, E., Kwak, L.M., and Zartman, R.E., 1987, U-Th-Pb and $^{40}Ar/^{39}Ar$ dating of the Mountain Pass carbonatite and alkali-igneous rocks, southeastern California: Geological Society of America Abstracts with Programs, v. 19, p. 542.

Dindi, E.W., and Swain, C.J., 1988, Joint three-dimensional inversion of gravity and magnetic data from Jombo Hill alkaline complex, Kenya: Journal of the Geological Society, v. 145, p. 493–504, https://doi.org/10.1144/gsjgs.145.3.0493.

Drenth, B.J., 2014, Geophysical expression of a buried niobium and rare earth element deposit: The Elk Creek carbonatite, Nebraska, USA: Interpretation (Tulsa), v. 2, no. 4, p. SJ169–SJ179, https://doi.org/10.1190/INT-2014-0002.1.

Fleck, R.J., Carr, M.D., Davis, G.A., and Burchfiel, B.C., 1994, Isotopic complexities and the age of the Delfonte volcanic rocks, eastern Mescal Range, southeastern California: Stratigraphic and tectonic implications: Geological Society of America Bulletin, v. 106, p. 1242–1253, https://doi.org/10.1130/0016-7606(1994)106<1242:ICATAO>2.3.CO;2.

Gamble, T.D., Goubau, W.M., and Clarke, J., 1979, Magnetotellurics with a remote magnetic reference: Geophysics, v. 44, p. 53–68, https://doi.org/10.1190/1.1440923.

Glover, P.W.J., 2010, A generalized Archie's law from phases: Geophysics, v. 75, p. E247–E256, https://doi.org/10.1190/1.3509781.

Godson, R.H., and Plouff, D., 1988, BOUGUER version 1.0, A microcomputer gravity-terrain-correction program: U.S. Geological Survey Open-File Report 88-644, https://doi.org/10.3133/ofr88644A and https://doi.org/10.3133/ofr88644B.

Grauch, V.J.S., and Cordell, L., 1987, Limitations of determining density or magnetic boundaries from the horizontal gradient of gravity or pseudogravity data: Geophysics, v. 52, p. 118–121, https://doi.org/10.1190/1.1442236.

Groves, D.I., and Vielreicher, N.M., 2001, The Phalabowra (Palabora) carbonatite-hosted magnetite copper sulphide deposit, South Africa: An endmember of the iron-oxide copper–gold–rare earth element group: Mineralium Deposita, v. 36, p. 189–194, https://doi.org/10.1007/s001260050298.

Hatch, G.P., 2012, Dynamics in the global market for rare earths: Elements, v. 8, p. 341–346, https://doi.org/10.2113/gselements.8.5.341.

Haxel, G.B., 2005, Ultrapotassic mafic dikes and rare earth element- and barium-rich carbonatite at Mountain Pass, Mojave Desert, southern California: Summary and field trip localities: U.S. Geological Survey Open-File Report 2005-1219, http://pubs.usgs.gov/of/2005/1219/.

Haxel, G.B., 2007, Ultrapotassic rocks, carbonatite, and rare earth element deposit, Mountain Pass, southern California, *in* Theodore, T.G., ed., Geology and Mineral Resources of the East Mojave National Scenic Area, San Bernardino County, California: U.S. Geological Survey Bulletin 2160, p. 17–55, https://doi.org/10.3133/b2160.

Haxel, G.B., Hedrick, J.B., and Orris, G.J., 2002, Rare earth elements—Critical resources for high technology: U.S. Geological Survey Fact Sheet 087-02, 4 p., https://pubs.usgs.gov/fs/2002/fs087-02/fs087-02.pdf.

Hendricks, J.D., 2007, Geophysics, *in* Theodore, T.G., ed., Geology and Mineral Resources of the East Mojave National Scenic Area, San Bernardino County, California: U.S. Geological Survey Bulletin 2160, p. 81–87, https://doi.org/10.3133/b2160.

Hewett, D.F., 1956, Geology and mineral resources of the Ivanpah quadrangle, California and Nevada: U.S. Geological Survey Professional Paper 275, 2 sheets, scale 1:125,000, https://doi.org/10.3133/pp275.

Kucks, R.P., Hill, P.L., and Ponce, D.A., 2006, Nevada magnetic and gravity maps and data: A website for the distribution of data: U.S. Geological Survey Data Series 234, https://doi.org/10.3133/ds234.

Kunetz, G., 1972, Processing and interpretation of magnetotelluric soundings: Geophysics, v. 37, p. 1005–1021, https://doi.org/10.1190/1.1440310.

Langenheim, V.E., Biehler, S., Negrini, R., Mickus, K., Miller, D.M., and Miller, R.J., 2009, Gravity and magnetic investigations of the Mojave National Preserve and adjacent areas, California and Nevada: U.S. Geological Survey Open-File Report 2009-1117, 25 p., http://pubs.usgs.gov/of/2009/1117/.

Long, K.R., Van Gosen, B.S., Foley, N.K., and Cordier, D., 2010, The principal rare earth elements deposits of the United States: A summary of domestic deposits and a global perspective: U.S. Geological Survey Scientific Investigations Report 2010-5220, 96 p., https://pubs.usgs.gov/sir/2010/5220/.

Mariano, A.N., and Mariano, A.J., 2012, Rare earth mining and exploration in North America: Elements, v. 8, p. 369–376, https://doi.org/10.2113/gselements.8.5.369.

Massari, S., and Ruberti, M., 2013, Rare earth elements as critical raw materials: Focus on international markets and future strategies: Resources Policy, v. 38, p. 36–43, https://doi.org/10.1016/j.resourpol.2012.07.001.

McCafferty, A.E., Stoeser, D.B., and Van Gosen, B.S., 2014, Geophysical interpretation of U, Th, and rare earth element mineralization of the Bokan Mountain peralkaline granite complex, Prince of Wales Island, southeast Alaska: Interpretation (Tulsa), v. 2, no. 4, p. SJ47–SJ63, https://doi.org/10.1190/INT-2014-0010.1.

McKinney, S.T., Cottle, J.M., and Lederer, G.W., 2015, Evaluating rare earth element (REE) mineralization mechanisms in Proterozoic gneiss, Music Valley, California: Geological Society of America Bulletin, v. 127, p. 1135–1152, https://doi.org/10.1130/B31165.1.

Miller, D.M., Miller, R.J., Nielsen, J.E., Wilshire, H.G., Howard, K.A., and Stone, P., compilers 2007, Geologic map of the East Mojave National Scenic Area, California, *in* Theodore, T.G., ed., Geology and Mineral Resources of the East Mojave National Scenic Area, San Bernardino County, California: U.S. Geological Survey Bulletin 2160, Plate 1, scale 1:125,000, https://doi.org/10.3133/b2160.

Moyle, W.R., Jr., 1972, Water wells and springs in Ivanpah Valley, San Bernardino County, California: California Department of Water Resources Bulletin 91-21, 56 p.

Olhoeft, G.R., 1985, Low-frequency electrical properties: Geophysics, v. 50, p. 2492–2503, https://doi.org/10.1190/1.1441880.

Olson, J.E., Shawe, D.R., Pray, L.C., and Sharp, W.N., 1954, Rare-earth mineral deposits of the Mountain Pass district, San Bernardino County, California: U.S. Geological Survey Professional Paper 261, 75 p., https://doi.org/10.3133/pp261.

Peacock, J.R., Mangan, M.T., McPhee, D., and Ponce, D.A., 2015, Imaging the magmatic system of Mono Basin, California, with magnetotellurics in three dimensions: Journal of Geophysical Research: Solid Earth, v. 120, p. 7273–7289, https://doi.org/10.1002/2015JB012071.

Peacock, J.R., Denton, K.M., and Ponce, D.A., 2016, Magnetotelluric imaging of a carbonatite terrane in the southeast Mojave Desert, California and Nevada: Australian Society of Exploration Geophysicists Extended Abstracts, v. 2016, 5 p., https://doi.org/10.1071/ASEG2016ab148.

Peacock, J.R., Denton, K.M., and Ponce, D.A., 2019, Magnetotelluric data of Mountain Pass, California: U.S. Geological Survey data release, https://doi.org/10.5066/P9JNPLPJ.

Phillips, F.M., 2003, Cosmogenic ^{36}Cl ages of Quaternary basalt flows in the Mojave Desert, California, USA: Geomorphology, v. 53, p. 199–208, https://doi.org/10.1016/S0169-555X(02)00328-8.

Phillips, J.D., 2001, Designing matched bandpass and azimuthal filters for the separation of potential-field anomalies by source region and source type: Australian Society of Exploration Geophysicists Extended Abstracts, v. 2001, 4 p., https://doi.org/10.1071/ASEG2001ab110.

Poletti, J.E., Cottle, J.M., Hagen-Peter, G.A., and Lackey, J.S., 2016, Petrochronological constraints on the origin of the Mountain Pass ultrapotassic and carbonatite intrusive suite, California: Journal of Petrology, v. 57, p. 1555–1598, https://doi.org/10.1093/petrology/egw050.

Ponce, D.A., 1997, Gravity data of Nevada: U.S. Geological Survey Digital Data Series 42, 27 p., CD-ROM, https://doi.org/10.3133/ds42.

Premo, W.R., DeWitt, E.H., Moscati, R.J., Stoeser, D., and Premo, V.L., 2013, Ages and Pb-Sr-Nd isotopes of silicate rocks at Mountain Pass, southern California: Geological Society of America Abstracts with Programs, v. 45, no. 7, p. 113.

Downloaded from https://pubs.geoscienceworld.org/gsa/geosphere/article-pdf/doi/10.1130/GES02066.1/4907657/ges02066.pdf
by guest

Ramberg, I.B., 1973, Gravity studies of the Fen Complex, Norway, and their petrological significance: Contributions to Mineralogy and Petrology, v. 38, p. 115–134, https://doi.org/10.1007/BF00373876.
Ray, G.E., and Lefebure, D.V., 2000, A synopsis of iron oxide ± Cu ± Au ± P ± REE deposits of the Candelaria-Kiruna-Olympic Dam family, *in* Geological Fieldwork 1999: British Columbia Ministry of Energy and Mines Paper 2000-1, p. 267–272.
Roberts, C.W., and Jachens, R.C., 1999, Preliminary aeromagnetic anomaly map of California: U.S. Geological Survey Open-File Report 99-440, 14 p., https://doi.org/10.3133/ofr99440.
Saltus, R.W., and Blakely, R.J., 2011, Unique geologic insights from non-unique gravity and magnetic interpretation: GSA Today, v. 21, no. 12, p. 4–10, https://doi.org/10.1130/G136A.1.
Shah, A.K., Bern, C.R., Van Gosen, B.S., Daniels, D.L., Benzel, W.M., Budahn, J.R., Ellefsen, K.J., Karst, A., and Davis, R., 2017, Rare earth mineral potential in the southeastern U.S. Coastal Plain from integrated geophysical, geochemical, and geological approaches: Geological Society of America Bulletin, v. 129, p. 1140–1157, https://doi.org/10.1130/B31481.1.
Shawe, D.R., 1953, Thorium resources of the Mountain Pass District, San Bernardino County, California: U.S. Geological Survey Trace Element Investigation Report 251, 58 p., https://doi.org/10.3133/tei251.
Simpson, R.W., Jachens, R.C., Blakely, R.J., and Saltus, R.W., 1986, A new isostatic residual gravity map of the conterminous United States with a discussion on the significance of isostatic residual gravity anomalies: Journal of Geophysical Research, v. 91, p. 8348–8372, https://doi.org/10.1029/JB091iB08p08348.
Stoeser, D.B., 2013, Mineralogy and late stage alteration of the Mountain Pass, California, ultrapotassic silicate intrusive rocks: Geological Society of America Abstracts with Programs, v. 45, no. 7, p. 500.
Syberg, F.J.R., 1972, A Fourier method for the regional-residual problem of potential fields: Geophysical Prospecting, v. 20, p. 47–75, https://doi.org/10.1111/j.1365-2478.1972.tb00619.x.
Tape, C., Plesch, A., Shaw, J.H., and Gilbert, H., 2012, Estimating a continuous Moho surface for the California unified velocity model: Seismological Research Letters, v. 83, p. 728–735, https://doi.org/10.1785/0220110118.
Theodore, T.G., 2007, Evaluation of metallic mineral resources, *in* Theodore, T.G., ed., Geology and Mineral Resources of the East Mojave National Scenic Area, San Bernardino County, California: U.S. Geological Survey Bulletin 2160, p. 187–195, https://doi.org/10.3133/b2160.
U.S. Geological Survey, 2015, Mineral commodity summaries 2015: Reston, Virginia, U.S. Geological Survey, 202 p., https://doi.org/10.3133/70140094.
Verplanck, P.L., and Van Gosen, B.S., 2011, Carbonatite and alkaline intrusion-related rare earth element deposits—A deposit model: U.S Geological Survey Open-File Report 2011-1256, 5 p., https://doi.org/10.3133/ofr20111256.
Walker, J.D., Burchfiel, B.C., and Davis, G.A., 1995, New age controls on initiation and timing of foreland belt thrusting in the Clark Mountains, southern California: Geological Society of America Bulletin, v. 107, p. 742–750, https://doi.org/10.1130/0016-7606(1995)107<0742:NACOIA>2.3.CO;2.
Wannamaker, P.E., 2005, Anisotropy versus heterogeneity in continental solid earth electromagnetic studies: Fundamental response characteristics and implications for physicochemical state: Surveys in Geophysics, v. 26, p. 733–765, https://doi.org/10.1007/s10712-005-1832-1.
Wannamaker, P.E., Hohmann, G.W., and Ward, S.H., 1984, Magnetotelluric responses of three-dimensional bodies in layered earths: Geophysics, v. 49, p. 1517–1533, https://doi.org/10.1190/1.1441777.
Wannamaker, P.E., Hasterok, D.P., Johnston, J.M., Stodt, J.A., Hall, D.B., Sodergren, T.L., Pellerin, L., Maris, V., Doerner, W.M., and Unsworth, M.J., 2008, Lithospheric dismemberment and magmatic processes of the Great Basin–Colorado Plateau transition, Utah, implied from magnetotellurics: Geochemistry Geophysics Geosystems, v. 9, Q05019, https://doi.org/10.1029/2007GC001886.
Wooden, J.L., and Miller, D.M., 1990, Chronologic and isotopic framework for Early Proterozoic crustal evolution in the eastern Mojave Desert region, southeastern California: Journal of Geophysical Research, v. 95, p. 20,133–20,145, https://doi.org/10.1029/JB095iB12p20133.
Woyski, M., 1980, Petrology of the Mountain Pass Carbonatite Complex: A review, *in* Fife, D.L., and Brown, A.R., eds., Geology and Mineral Wealth of the California Desert: South Coast Geological Society, p. 357–378.

Downloaded from https://pubs.geoscienceworld.org/gsa/geosphere/article-pdf/doi/10.1130/GES02066.1/4907657/ges02066.pdf
by guest